APL Photonics

Integration of Brillouin and passive circuits for enhanced radio-frequency photonic filtering

Cite as: APL Photonics 4, 106103 (2019); https://doi.org/10.1063/1.5113569
Submitted: 05 June 2019 . Accepted: 18 September 2019 . Published Online: 03 October 2019

Yang Liu, Amol Choudhary, Guanghui Ren, Khu Vu, Blair Morrison, Alvaro Casas-Bedoya, Thach G. Nguyen, Duk-Yong Choi, Pan Ma, Arnan Mitchell, Stephen J. Madden, David Marpaung, and Benjamin J. Eggleton

AIP Publishing

Integration of Brillouin and passive circuits for enhanced radio-frequency photonic filtering

Cite as: APL Photon. 4, 106103 (2019); doi: 10.1063/1.5113569
Submitted: 5 June 2019 • Accepted: 18 September 2019 •
Published Online: 3 October 2019

Yang Liu,[1,2,a] Amol Choudhary,[1,2,b] Guanghui Ren,[3] Khu Vu,[4] Blair Morrison,[1,2,c] Alvaro Casas-Bedoya,[1,2] Thach G. Nguyen,[3] Duk-Yong Choi,[4] Pan Ma,[4] Arnan Mitchell,[3] Stephen J. Madden,[4] David Marpaung,[1,2,d] and Benjamin J. Eggleton[1,2]

AFFILIATIONS

[1]Institute of Photonics and Optical Science (IPOS), School of Physics, The University of Sydney, Sydney, NSW 2006, Australia
[2]The University of Sydney Nano Institute (Sydney Nano), The University of Sydney, Sydney, NSW 2006, Australia
[3]School of Engineering, RMIT University, Melbourne, VIC 3001, Australia
[4]Laser Physics Centre, Australian National University, Canberra, ACT 2601, Australia

Note: This article is part of the Special Topic on Hybrid Integration beyond Silicon Photonics.

[a]yang.liu@sydney.edu.au
[b]**Present address:** The Department of Electrical Engineering, Indian Institute of Technology, Delhi, India.
[c]**Present address:** Xanadu, Toronto, ON M5G 2C8, Canada.
[d]**Present address:** Laser Physics and Nonlinear Optics (LPNO), MESA+ Institute, University of Twente, 7522 NB Enschede, The Netherlands.

ABSTRACT

Signal processing using on-chip nonlinear or linear optical effects has shown tremendous potential for RF photonic applications. Combining nonlinear and linear elements on the same photonic chip can further enable advanced functionality and enhanced system performance in a robust and compact form. However, the integration of nonlinear and linear optical signal processing units remains challenging due to the competing and demanding waveguide requirements, specifically the combination of high optical nonlinearity in single-pass waveguides, which is desirable for broadband signal processing with low linear loss and negligible nonlinear distortions required for linear signal processing. Here, we report the first demonstration of integrating Brillouin-active waveguides and passive ring resonators on the same integrated photonic chip, enabling an integrated microwave photonic notch filter with ultradeep stopband suppressions of >40 dB, a low filter passband loss of <−10 dB, flexible center frequency tuning over 15 GHz, and reconfigurable filter shape. This demonstration paves the way for implementing high-performance integrated photonic processing systems that merge complementary linear and nonlinear properties, for advanced functionality, enhanced performance, and compactness.

I. INTRODUCTION

On-chip nonlinear optical effects have been demonstrated as an attractive candidate to generate, convert, and process optical signals,[1] providing the unprecedented capability for manipulating microwave signals with enhanced functionalities and superior performance.[2,3] This enabling technology has been the basis of demonstrating low-noise microwave signal generation[4,5] and modulation,[6,7] broadband microwave signal mixing and measurement,[8,9] and compact multitap-based microwave filtering.[10,11]

Stimulated Brillouin Scattering (SBS),[12] one of the strongest nonlinear optical effects traditionally investigated in optical fibers, can induce an optical gain resonance with tens-of-MHz linewidth over the broadband frequency range,[13,14] which is particularly attractive for microwave signal processing, enabling the desired MHz-level spectral resolution, and ultrawideband tunability. Recently, achievements in harnessing SBS in centimeter-scale photonic circuits[15–17] have shown advanced microwave photonic (MWP) functionalities including on-chip narrowband filtering,[18–22] compact time delay,[23,24] broadband phase shifters,[25,26] and chip-based RF

signal generation.[5,27] Although novel on-chip MWP functionalities have been reported using complex modulation configurations, the RF link performance of these schemes is limited by the broadband destructive RF interference, typically resulting in high RF insertion losses.[18,23,28]

To unleash the full potential of the on-chip Brillouin signal processing, it is desirable to combine Brillouin-active circuits with conventional functional linear integrated photonic devices, particularly integrated ring resonators that provide flexibly tailored phase and amplitude responses for photonic signal processing.[29–32] This principle has been demonstrated by pairing the optical responses of a Brillouin gain resonance in a 4.6-km-long optical fiber with an integrated ring resonator. This scheme yielded a high-performance microwave photonic (MWP) notch filter using a simple MWP link based on standard intensity modulation and direct photodetection, enabling the combination of ultrahigh suppression, lossless RF passbands, and programmable filter shapes.[33] However, the on-chip integration of Brillouin-active and linear circuits remains challenging, as the demanding material requirements including low optical loss and high optical nonlinearity for Brillouin processing and linear optical processing must be simultaneously satisfied.[34]

In this work, we present high-performance integrated MWP (IMWP) signal processing based on a centimeter-scale photonic circuit that pairs the Brillouin processor with passive functional devices. We implement an IMWP notch filter scheme using an integrated As_2S_3 photonic chip that consists of a Brillouin-active element and an overcoupled ring resonator, which can provide separate nonlinear and linear optical signal processing functionalities. Using this As_2S_3 photonic chip, a highly localized π-phase inversion can be formed by cascading the complementary optical responses of the Brillouin gain resonance and the ring resonance, leading to an RF notch response due to the localized RF destructive interference. This on-chip implementation enables a new class of IMWP devices that are compact and robust, while exhibiting desirable advantages of deep filter rejection, high resolution, filter shape tunability, and the compatibility with simple MWP link configuration.

II. ILLUSTRATION OF CONCEPT

Figure 1(a) shows the architecture of the IMWP processors based on pairing linear functional devices with Brillouin-active circuits. Figure 1(b) illustrates the integrated photonic circuit that enables the high-performance IMWP notch filter demonstrated in this work. By appropriately setting the optical pump wavelength, the Brillouin-active waveguide can be selectively activated to provide a gain resonance, while the ring resonator only operates as passive optical filtering devices without nonlinear distortion. Combining the optical responses of the active Brillouin process and passive ring resonance can synthesize a unique optical response that is critical to implement an enhanced microwave photonic notch filter.

The principle of the filter scheme is constructing a localized π phase-shift-only optical response, using the complementary optical responses of an OC ring resonator and SBS responses. The localized π phase inversion and unchanged amplitude on one optical sideband will form a localized destructive RF interference via direction photodetection, as shown in Fig. 2. To describe the filter response formation, we consider that the upper sideband of intensity-modulated

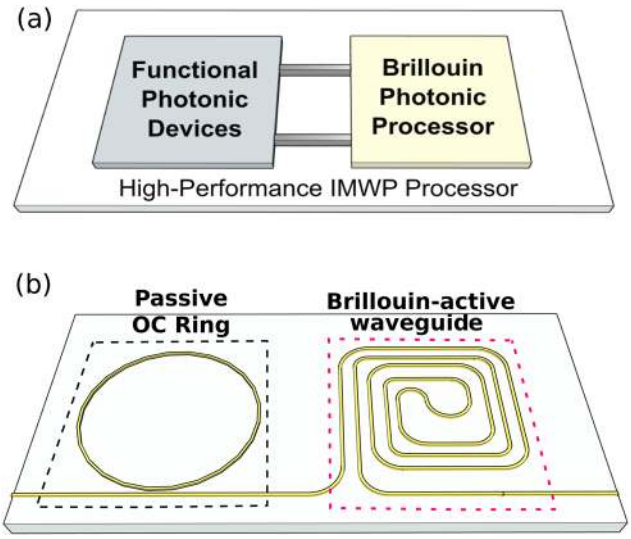

FIG. 1. (a) Architecture of a new class of IMWP processors that integrates a Brillouin photonic processor and functional photonic devices on the same photonic chip, providing enhanced performance and unique functionality. (b) Architecture of the IMWP notch filter demonstrated in this work, consisting of an overcoupled (OC) ring resonator interconnected with a Brillouin waveguide providing SBS gain resonance. The dashed boxes indicate the passive OC ring resonator and the nonlinear Brillouin-active waveguide, separately.

optical signals is processed by an optical response $H_{opt}(\omega)$. Via photodetection, the RF signal (photocurrent) is given by[35]

$$H_{RF}(\omega_{RF}) \propto \cos(\omega_{RF}t) + \cos(\omega_{RF}t + \phi_{opt})|H_{opt}(\omega_c + \omega_{RF})| \propto \sqrt{1 + |H_{opt}|^2 + 2|H_{opt}|\cos\phi_{opt}}\cos(\omega_{RF}t + \phi_{RF}), \quad (1)$$

where $H_{opt}(\omega_c + \omega_{RF})$ is the applied optical response at $\omega_c + \omega_{RF}$ in the optical domain, ω_c is the optical carrier frequency, and ω_{RF} is the RF frequency. Equation (1) implies the condition to implement a null response in the RF domain, given by

$$H_{RF}(\omega_{RF}) = \begin{cases} 0, & \text{if } \phi_{opt} = \pi \ \& \ |H_{opt}(\omega_c + \omega_{RF})| = 1, \\ \neq 0, & \text{otherwise.} \end{cases} \quad (2)$$

Thus, the key to implement an RF filter notch function is to find a unique optical response, producing a π phase shift without altering amplitude at the same frequency. However, it is challenging to find on-chip photonic devices that can directly generate such a unique optical response. To bypass this limit, we introduce a hybrid filter concept that constructs the desired optical response by cascading the transfer functions of two optical devices, which can be mathematically described by

$$H_{opt}(\omega) = H_{opt,1}(\omega) \cdot H_{opt,2}(\omega), \quad (3)$$

where the optical response $H_{opt,1}(\omega)$ is generated by an overcoupled ring resonator and $H_{opt,2}(\omega)$ is produced by the SBS gain resonance in this work.

The approach to synthesizing the desired optical response and filter response formation is illustrated in Fig. 3. The input RF signal is encoded in the optical domain through intensity modulation,

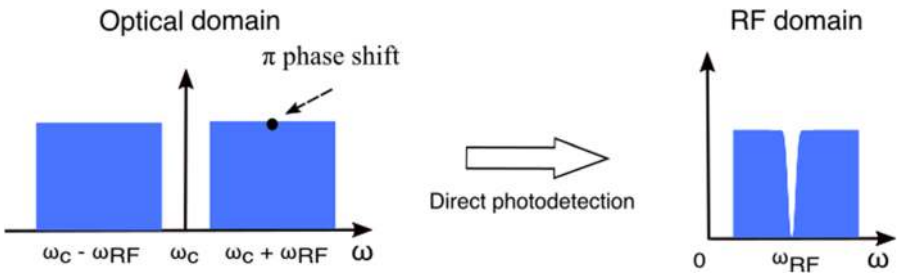

FIG. 2. Schematic illustrations of the implementation of the RF photonic filter based on the SSB modulation scheme, with only one optical sideband being processed. When a π-phase-shit only optical response is applied to the optical upper sideband, a notch response forms in the RF domain via direct photodetection.

forming dual in-phase optical sidebands with equal amplitudes, as shown by the spectrum diagram at spot ***A*** in the MWP filter link. The modulated optical signal is sent to the integrated photonic circuit for optical sideband processing. An overcoupled (OC) ring resonator processes the upper sideband at the frequency of $\omega_c + \omega_{RF}$, generating an optical response $H_{opt,1}(\omega)$ of amplitude suppression and a 0-to-2π phase transition (π-phase inversion at the resonance frequency), as shown by the spectrum diagram at ***B***.

Subsequently, a counterpropagating optical pump is injected into the photonic chip through the other end facet to induce SBS gain resonance. The induced Brillouin gain resonance produces an optical gain resonance $H_{opt,2}(\omega)$ centered at the frequency of $\omega_c + \omega_{RF}$. The SBS gain resonance imparts amplitude amplification to balance the amplitude suppression induced by the ring resonance $H_{opt,1}(\omega)$. As a result, the sideband amplitudes at $\omega_c - \omega_{RF}$ and $\omega_c + \omega_{RF}$ will be equalized, as illustrated by the spectrum diagram at ***C***. A small phase response is also introduced by the SBS gain, but it does not change the π-phase inversion at $\omega_c + \omega_{RF}$. By cascading these two optical responses, a synthesized transfer function $H_{opt}(\omega) = H_{opt,1}(\omega) \cdot H_{opt,2}(\omega)$ can be constructed, exhibiting a π-phase-shift-only response at the frequency of interest. It should be noted that the SBS pump is located outside the ring resonator's resonance frequency so that the SBS process is activated only in the spiral waveguide and is avoided in the ring resonator. Thus, the SBS gain process only occurs in the spiral waveguide, which amplifies the counter-propagating optical signal that has been processed by the ring resonator.

The processed optical signal is transmitted out from the photonic circuit and is collected by a photodetector. Via direct photodetection, an ultradeep notch at ω_{RF} in the RF domain is formed due to the localized destructive RF interference at the frequency of ω_{RF}. This RF cancellation occurs since the optical sideband amplitudes

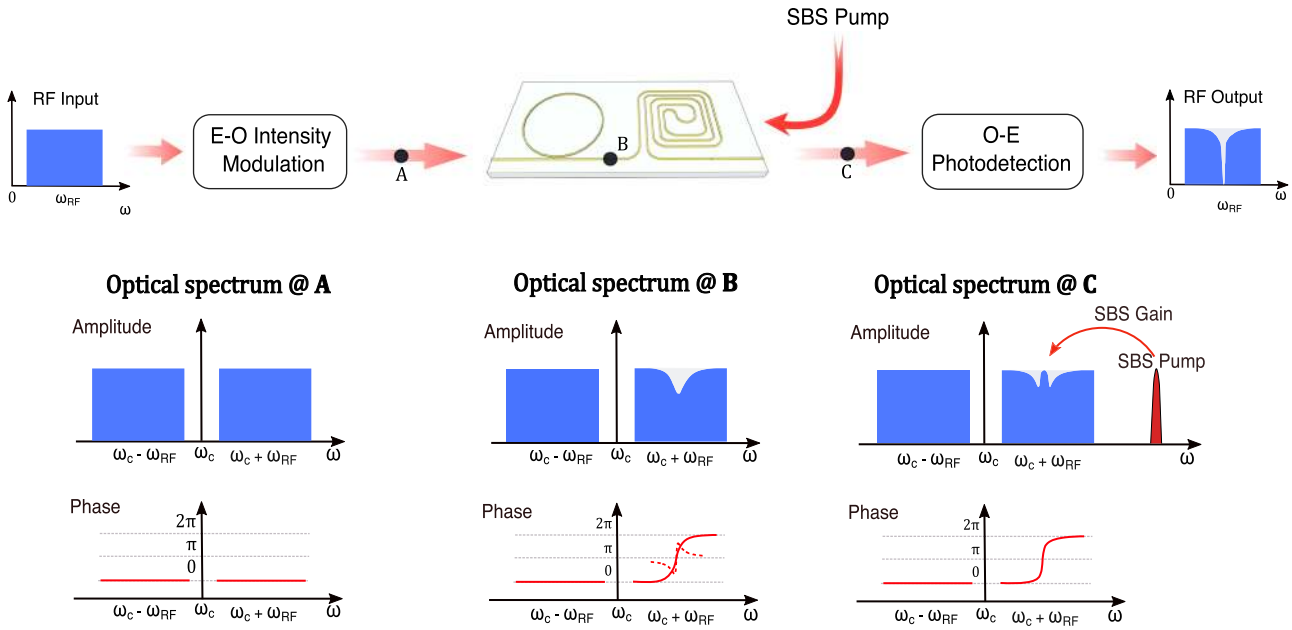

FIG. 3. Schematic of the implementation of an IMWP notch filter. An integrated chip with overcoupled (OC) ring resonator and Brillouin-active waveguide is embedded in an MWP link using intensity modulation and direction photodetection. The spectrum diagrams illustrating amplitude and phase responses at different positions denoted by **A**, **B**, and **C** in the link are illustrated. At location **B**, the phase response denoted in the dashed curve is induced by the SBS gain resonance. The SBS-induced phase response adds up with the phase response generated by the OC ring resonator, resulting in a steeper phase response denoted by the spectrum at location **C**. E–O: electrical-to-optical conversion and O–E: optical-to-electrical conversion.

are matched but with a π-phase difference between two sidebands at $\omega_c \pm \omega_{RF}$. In contrast, constructive RF interference is formed in the RF passband due to the in-phase optical passbands.

III. PHOTONIC CIRCUIT DESIGN AND FABRICATION

The integration of both the passive ring resonator and the Brillouin-active units on the same photonic chip is challenging, as it raises the requirements of an integrated platform that yields low losses, efficient SBS gain, and low nonlinear absorption losses. Fortunately, the integrated As_2S_3 photonic chip offers a promising platform to accommodate both efficient SBS-active circuits and low-loss passive devices. In this section, the design of the key devices and the fabrication process of the integrated As_2S_3 photonic circuit are discussed.

A. Design of nonlinear Brillouin-active waveguide

To achieve efficient optoacoustic interactions in the on-chip SBS process, a high optic-acoustic field overlap is required.[15,36,37] This requirement translates into the simultaneous confinement of acoustic and optical waves in the same waveguide structure. To this end, the waveguide core material is expected to have a higher refractive index to achieve optical wave guidance, while its mechanical property needs to be softer than the cladding material.[36] As a result, both the optical wave and the acoustic wave travel at a lower speed in the core area, compared to a higher speed in the cladding, as schematically illustrated in Figs. 4(a) and 4(b).

The waveguide structure consisting of an As_2S_3 core and SiO_2 claddings is an ideal scheme to simultaneously guide the acoustic and optical waves in the same waveguide. The high contrast in both refractive index and acoustic velocity offers tight optical and acoustic confinements, leading to strong optoacoustic interactions. Figure 4(c) shows the numerical simulation of a fundamental optical mode (TE_0) in an As_2S_3-SiO_2 waveguide with a cross section of 1.9 μm by 0.68 μm. Figure 4(d) shows the numerical simulation of an acoustic mode that yields the highest mode overlap with the fundamental optical mode based on a finite element analysis method.[38] In contrast to the optical mode, the acoustic mode pattern indicates that the acoustic waveguide is heavily multimodal. This is due to the fact that the acoustic wavelength is around 340 nm, much less than the waveguide core dimension. However, this acoustic mode with a symmetric field distribution is still able to provide an efficient field overlap with the optical field, achieving a large SBS gain coefficient. Complete material parameters of As_2S_3 and SiO_2 mechanical properties used in the numerical simulations can be found in the reported work by Smith *et al.*[39]

In this waveguide, the simulated SBS gain spectrum is shown in Fig. 5, exhibiting a SBS gain coefficient around 600 m^{-1} W^{-1}. One can find that the FWHM linewidth of the predominant Brillouin gain peak is around 40 MHz, which is the inverse of the acoustic lifetime (typically ~10 ns). There also exhibit small gain peaks in adjacent to the main peak, which are induced by the other acoustic waves that yield a much smaller mode overlap with the optical mode. In the waveguide design of this work, the trade-off between the waveguide width and the gain coefficient needs to be considered, as narrower widths with stronger side-wall scattering will lead to a higher propagation loss that can in turn reduce the SBS gain.

B. Design of linear overcoupled ring resonator

To obtain the desired π phase shift, it is critical to achieving a ring resonator operated in the overcoupled regime with low losses. Figure 6(a) shows the schematic topology of the OC ring resonator using the As_2S_3 material. The OC ring resonator is designed to have a circumference of 4.7 mm, producing a free spectral range (FSR) of ~30 GHz. The waveguide width of the ring resonator is 2.6 μm, which is larger than the width (1.9 μm) of the bus waveguide. The larger width of the ring is used to reduce the optical propagation loss caused by the waveguide sidewall scattering.[40–42] A directional coupler with a length of 150 μm is used in the coupling regime in the ring resonator to enable efficient optical coupling between the bus waveguide and the ring resonator. The waveguide thickness for the entire chip is optimized to 0.68 μm, taking into account the waveguide loss and optical mode numbers. In practical fabrication, a spiral topology is used to achieve a compact footprint of the ring resonator, with an optimized spline bend radius of 30.2 μm.

The waveguide width of the directional coupler is designed as 0.85 μm, as shown in Fig. 6(b). The narrower waveguide width can

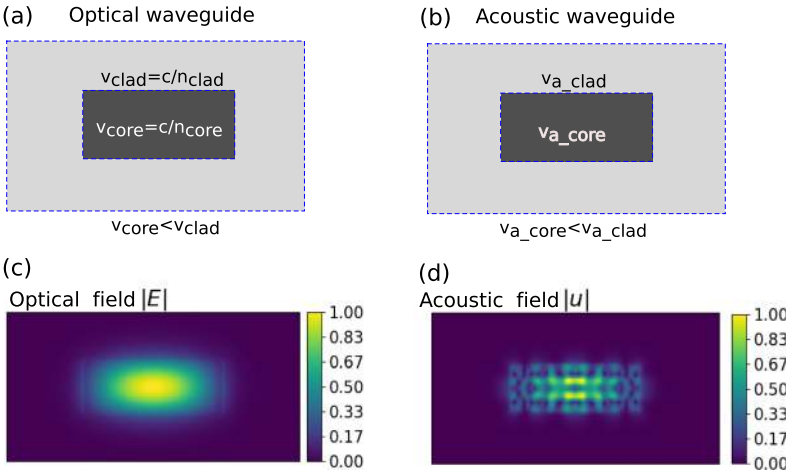

FIG. 4. The schematics of the cross section and wave velocity relationships for (a) the optical wave and (b) the acoustic wave, respectively. In the numerical simulation, the waveguide core and cladding material are set as As_2S_3 and SiO_2, respectively. The optical refractive indices for As_2S_3 and SiO_2 are set 2.44 and 1.45 in the numerical simulations, respectively. The cross section is set to have a width of 1.9 μm and a thickness of 0.68 μm. (c) The fundamental TE_{00} optical mode and (d) the acoustic mode of a dominant longitudinal sound wave are presented, separately. The field amplitude is normalized for better visibility.

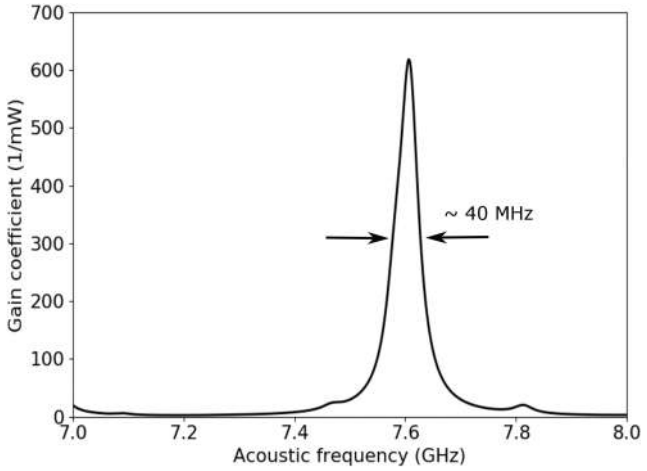

FIG. 5. A typical gain spectrum of backward SBS in the As_2S_3 waveguide surrounded by a SiO_2 cladding, with a width of 1.9 μm and a thickness of 0.68 μm.

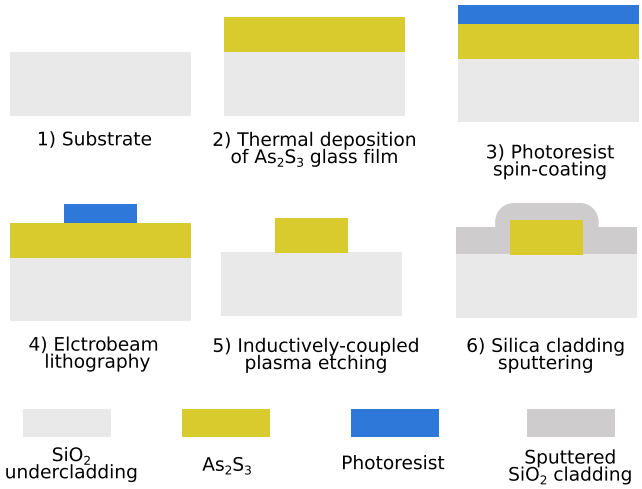

FIG. 7. Schematic of the fabrication process of the As_2S_3 waveguide.

provide stronger coupling between the two identical waveguides due to the strong evanescent optical fields of the narrow waveguides. In the meantime, the coupler waveguide in the ring resonator can be used as a modal stripper to filter out the higher-order optical modes, since 0.85 μm is close to the cutoff width for higher-order optical modes. Controlling the cross coupling coefficient between the ring resonator and the bus waveguide is the key to manipulate the coupling state of the ring resonator. To find an optimized coupler gap to enabled over coupling, numerical calculations were performed to predict the cross coupling strength. According to the coupled-mode theory,[43–45] the power coupling ratio, i.e., the fraction of the coupled power to the other waveguide, is given by

$$t^2 = \frac{P_{coupled}}{P_0} = \sin^2(C \cdot L), \tag{4}$$

where $P_{coupled}$ is the coupled power with an input optical power of P_0, L is the coupler length, and C is the coupling coefficient given by

$$C = \frac{\pi \Delta n_{eff}}{\lambda}, \tag{5}$$

where λ is the optical wavelength and Δn_{eff} is the effective refractive index difference of the symmetric and asymmetric supermodes.

Using numerical simulations, Δn_{eff} can be obtained for the waveguide cross section shown in Fig. 6(b). Using Eqs. (4) and (5), the power coupling ratio as a function of the coupler gap is calculated, as shown in Fig. 6(c). Using the measured waveguide propagation loss α_{dB} of 0.7 dB/cm, the power round-trip loss (the power loss ratio) is denoted by the dashed line. This dashed line intersects with the curve of the coupling strength at the coupler gap of 630 nm, indicating a critical point for the coupling state of the ring resonator. When the coupling is stronger than the round-trip loss, the ring is operated in the OC regime. Therefore, the coupler gap needs to be smaller than 630 nm. In this work, the coupler gap is designed as 550 nm to achieve strong coupling over a coupler length of 150 μm.

C. Photonic circuit fabrication

Figure 7 illustrates the fabrication process of the As_2S_3 photonic circuit used in this work. The As_2S_3 thin film was deposited via thermal evaporation. The As_2S_3 thin film was deposited on a thermal oxide silicon wafer. The total film thickness was 680 nm, with a thickness uniformity of less than 1%. The waveguide pattern was printed using electron-beam lithography. The As_2S_3 waveguides were fully etched by the inductively coupled plasma dry

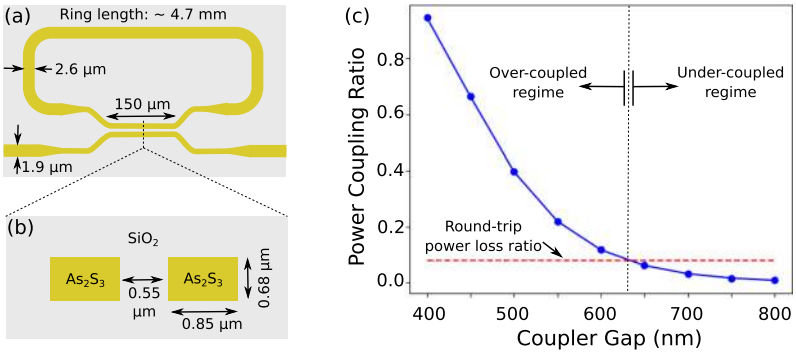

FIG. 6. Schematics of (a) the OC ring resonator and (b) the cross section of the directional coupler in the ring resonator. The feature sizes of each critical part of the ring resonator are marked. (c) The simulated coupling strength of the directional coupler with a coupling length of 150 μm.

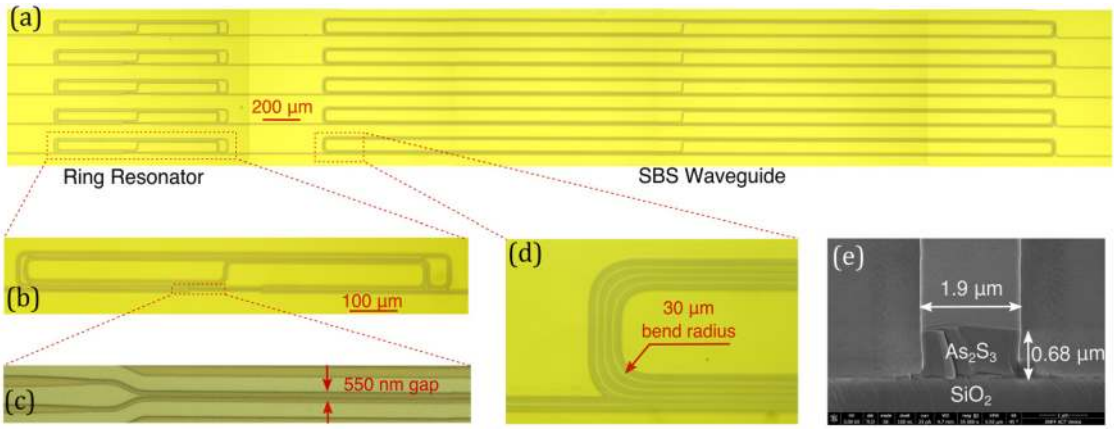

FIG. 8. Microscope images of (a) an array of the OC ring resonator cascaded with subsequent SBS spiral waveguides on the As_2S_3, (b) an OC ring resonator, (c) the zoomed-in directional coupler with 0.85-μm-wide waveguides of the resonator for light coupling, and (d) the waveguide bends in the SBS spiral waveguide. (e) A scanning electron microscopy (SEM) image of the cross section of the 1.9-μm-wide As_2S_3 waveguide before the silica upper cladding was sputtered.

etching technique using a mixture of CHF_3. A 1-μm-thickness SiO_2 upper-cladding was deposited via the sputtering process[46] to provide waveguide protection and acoustic confinement.

Figure 8(a) shows the microscope image of the fabricated As_2S_3 photonic chip consisting of an array of devices. Each device incorporates a ring resonator followed by a 4-cm-long Brillouin spiral waveguide. The ring resonators and Brillouin-active waveguides are designed in a spiral form to increase footprint compactness. Figures 8(b) and 8(c) show one of the ring resonators and the directional coupler in the coupling region, respectively. The coupler length, the waveguide width, and the coupler gap follow the dimension suggested by the design in Sec. III B. The adiabatic tapers were used to reduce the transition loss from the 2.6-μm wide ring waveguide to the few-mode waveguide in the directional coupler.

The ring resonator has a total length of ~4.7 mm, resulting in a measured free-spectral range of ~30 GHz. Waveguide bends with a radius of 30.2 μm are used in the spiral SBS waveguides, as shown in Fig. 8(d). The bend radius of the spline bends is linearly changed as a function of the bend length, which allows for adiabatic optical mode propagation with minimized radiation losses and optical mode cross coupling.[47] The SBS waveguides with a cross section size of 1.9 μm × 0.68 μm allow for efficient SBS gain and low optical propagation losses, as shown by the scanning electron microscopy (SEM) image in Fig. 8(e). Waveguides with the same size are also used for on-chip interconnection and routing to both ends of the chip for the end-fire optical coupling. The overall insertion loss of the Brillouin chip is ~18 dB, consisting of coupling losses of ~7 dB per facet and an overall propagation loss of ~1 dB/cm (including the bend losses).

IV. RESULTS

This section presents the on-chip device characterization, filter function implementation, and the link performance evaluation based on the aforementioned design principle and fabricated device.

A. Device characterization

Figure 9(a) shows the amplitude and phase responses of the OC ring resonator. The ring resonator exhibits a 3-dB linewidth of ~3 GHz, indicating a loaded Q factor of ~0.5×10^5. The phase response of the OC ring shows a phase transition from 0 to 2π with a π phase shift at the resonance frequency. These measured results indicate that the ring resonator is operated in the OC state, as predicted by the numerical calculations shown in Fig. 6(c). Figure 9(b) presents the measured responses of the SBS gain resonance. The dominant gain peak shows an SBS gain of ~12 dB and a maximum degree phase shift of ±40, at an optical pump power of 150 mW. A higher SBS gain beyond 20 dB can be achieved using a higher pump power. However, the maximum gain is limited by the highest pump power of around 400 mW that can cause heat damage. The existence of auxiliary SBS gain peaks at adjacent frequencies is induced by different acoustic waves in the waveguide. Here, we mainly focus on the optical response generated by the dominant gain peak. The SBS gain coefficient of the dominant peak is experimentally characterized, showing a gain coefficient of ~650 m^{-1} W^{-1}. The gain coefficient is in line with the reported results of As_2S_3 waveguides of the same dimension.[48]

Figures 9(a) and 9(b) show that the OC ring resonator and the SBS gain resonance exhibit complementary optical responses. The OC ring produces amplitude suppression, while the SBS gain resonance amplifies the amplitude. On the other hand, the OC ring shows a π phase shift at the resonance frequency, while the phase response at the SBS resonance frequency is zero. These complementary optical resonances can be superposed to synthesize the desired optical response discussed in Sec. II, producing the desired optical response $H_{opt}(\omega)$ that satisfies Eq. (2). However, there exists a large mismatch in the 3-dB bandwidths of the OC ring resonator (~3 GHz) and the SBS gain response (~40 MHz). This is different from the demonstration using ultralow-loss Si_3N_4 chip and km-long optical fiber,[49] in which the optical fiber allows for broadband SBS gain using the frequency-broadened optical pump to match the bandwidth of the OC Si_3N_4 ring resonance (hundreds of

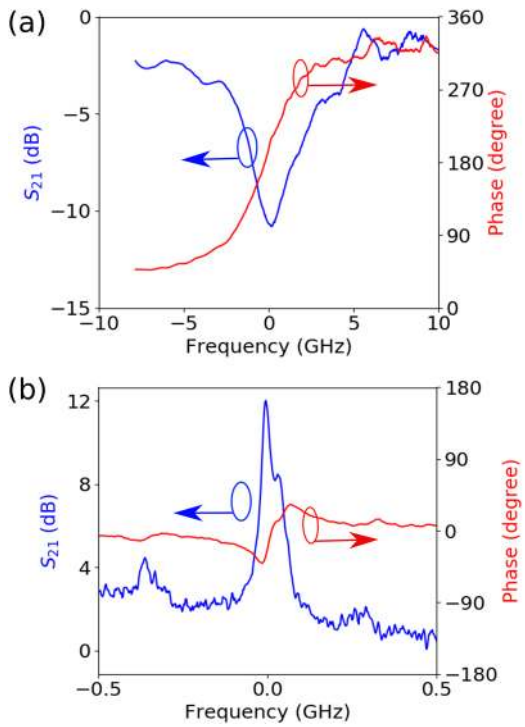

FIG. 9. Measured S_{21} responses of (a) the OC ring resonator and (b) the SBS gain resonance around the optical wavelength of 1550 nm. The frequency in the x-axis is normalized to the resonance frequency. Measured gain coefficient of the dominant gain peak at lower frequency down shifted from the optical pump frequency by 7.6 GHz.

megahertz). In this work, the current As_2S_3 chip is not able to provide broadband gain to compensate the amplitude suppression induced by the OC ring resonator. This is mainly limited by the relatively high waveguide loss (1 dB/cm) in the current sample. The waveguide propagation loss was derived from the measurements of the optical transmission losses of 1.9-μm-wide waveguides with different physical lengths. The measurement revealed an average propagation loss of 1 dB/cm, with a minimum propagation loss of 0.75 dB/cm. The Brillouin gain was constrained by the limited effective length of 2.6 cm of the As_2S_3 waveguide due to the relatively high optical propagation loss of 1 dB/cm and the short physical waveguide length of 4 cm. Such a high optical propagation loss was mainly limited by a larger sidewall roughness of the strip waveguide, compared with the conventional ridge waveguide. As a result, the bandwidth mismatch of two optical responses will lead to a broader 3-dB bandwidth of the synthesized MWP notch filter.

The large bandwidth of the synthesized filter response can be reduced using lower-loss ridge waveguide design which allows for reduced OC ring bandwidth and enhanced SBS gain. A lower optical propagation loss of <0.5 dB/cm has been achieved in previous work, using a wider As_2S_3 waveguide and a ridge waveguide cross section.[50] With the 0.5 dB/cm propagation loss and a length of 4.7 mm, a ring resonance operated in the overcoupled regime produces a FWHM bandwidth of ~650 MHz with a rejection of ~10 dB, exhibiting significantly bandwidth reduction from 3 GHz. On the other hand, the effective length of spiral As_2S_3 waveguides can be increased by more than two times, using such a low propagation loss and a waveguide length of >10 cm, which allows for a Brillouin gain of >30 dB under the same optical pump power. With such Brillouin gain capability, the SBS gain response can be broadened over the 200 MHz range to compensate the ring-induced amplitude suppression, approaching to the FWHM bandwidth of ~650 MHz of the overcoupled ring resonator. In the ongoing fabrication development, the propagation loss of As_2S_3 waveguides is promising to be pushed to a lower level of 0.2 dB/cm by reducing the sidewall roughness, which can produce a ring resonance resolution of ~200 MHz that can pair with the broadened Brillouin gain response.

B. Experimental implementation of the MWP notch filter

Figure 10 shows the experimental setup to implement the chip-based MWP notch filter based on the principle illustrated in Fig. 3. The output of the signal laser (laser 1) is intensity-modulated by the RF output of the vector network analyzer (VNA), generating two in-phase optical sidebands with the same amplitudes. After being amplified by an optical amplifier, the polarization of the modulated optical signal is adjusted by the polarization controller, which allows for efficient light coupling into the integrated photonic circuit. An optical isolator is used to prevent the back reflection of the optical signal at the chip facet. On the other hand, a continuous-wave

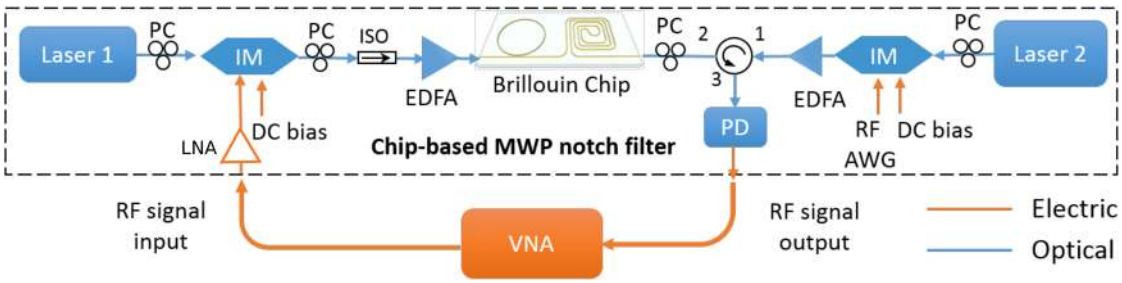

FIG. 10. Experimental implementation of the chip-based MWP notch filter with all the components contained in the dashed box. PC: polarization controller; ISO: isolator; EDFA: Er-doped fiber amplifier; AWG: arbitrary waveform generator; VNA: vector network analyzer; and LNA: low-noise RF amplifier.

optical pump generated by the pump laser (laser 2) is subsequently amplified by an optical amplifier. A circulator is used to separate the counter-propagating signal and pump waves. After passing through port 1 of the optical circulator, the counter-propagating optical pump is coupled to the chip via port 2 to induce SBS gain resonance. The lasers used in the experiment are operated at wavelengths near 1550 nm and can be tuned over the 50 GHz range, with a narrow linewidth of <1 MHz (Teraxion, LM).

The upper sideband of the modulated optical signal is processed by cascaded optical responses generated by the OC ring resonator and the SBS response, following the scheme illustrated in Fig. 3. The processed optical signal coming out from the photonic circuits is collected by a photodetector (Finisar HPDV2120R, 0.55 A/W responsivity), after being routed from port 2 to port 3 of the circulator. In the end, the detected RF signal is analyzed by the VNA. A second intensity modulator is used to generate multiple SBS pump teeth by producing additive optical sidebands. An RF signal generator outputs RF tones that determine the frequency intervals and the total frequency span of the optical pump lines. The use of pump broadening enables the formation of broader stopband RF filter response, satisfying the condition indicated by Eq. (2) over a broader frequency range.

In the experiment, an RF notch filter response was formed by pairing the complementary optical responses shown in Figs. 9(a) and 9(b). As shown in Fig. 11(a), with a single-frequency optical pump, RF filter responses with a single notch suppression of more than 40 dB are synthesized, as the perfect destructive interference merely occurs at the single frequency. However, the 3-dB bandwidth of the synthesized RF notch responses is ~3 GHz, limited by the OC ring resonance. By simply tuning the signal laser frequency (laser 1), the center frequency of the RF notch filter can be easily tuned from 0 to 15 GHz. The roll-off baseline of the filtering responses is attributed to the decaying responses of the RF components in the MWP filter link when the RF frequency increases. The central frequency tuning range is limited by half of the ring resonator's FSR (~30 GHz), taking into account the periodic ring resonance imparted on the other sideband. The frequency tuning range can be further increased by using rings with a shorter circumference. The center frequency tuning is achieved without tuning the resonance frequencies of the ring resonator or SBS response. This flexible tunability outperforms the RF photonic filters relying on dual-sideband processing.[51,52] Although the MWP filter based on single-sideband modulation can achieve the same level of tuning flexibility, but implementing single-sideband modulation causes increased system complexity and signal losses due to the use of additional sideband filtering. The RF photonic filter scheme demonstrated here completely eliminates these issues, benefiting from the synthetic combination of linear and nonlinear optical responses.

Since the SBS response can be optically programmable,[53,54] the MWP filter response can be reconfigured by simply adding more pump lines. In the experiment, by feeding an RF tone with a frequency of 80 MHz to the intensity modulator in the pump side, the modulated optical pump generates two optical sidebands symmetrically locating at both sides of the pump laser frequency. By tuning the DC bias of the intensity modulator, the amplitudes of the optical pump carrier and two sidebands can be equalized. As a result, a broader SBS response will be induced by the generated three pump lines with a frequency interval of 80 MHz.

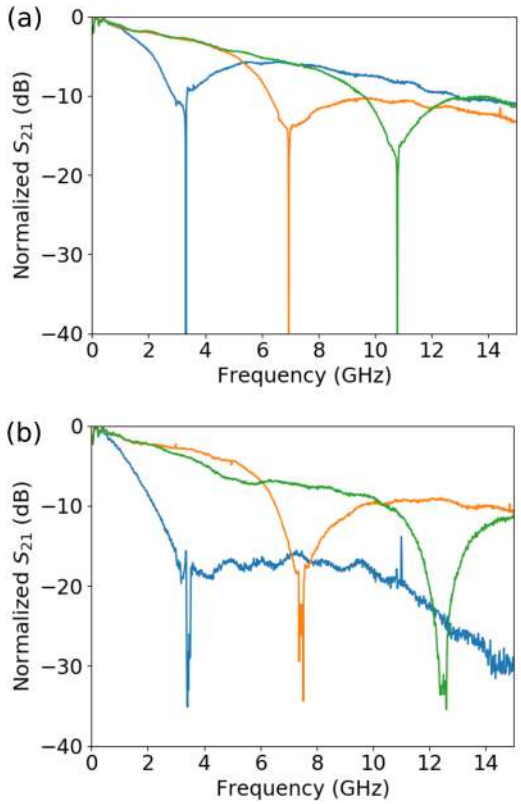

FIG. 11. Measured filter responses of (a) MWP notch filters and (b) MWP bandstop filters at different center frequencies with a 20-dB bandwidth of 100 MHz. The bandstop filter response was formed by using three optical pump lines with a frequency interval of 80 MHz. The filters responses are normalized to the maximum RF link gain at the lower frequencies.

The broadened SBS gain response will be superposed with the optical response of the OC ring resonator. Therefore, a bandstop filter response can be implemented, also with a frequency tunability over 15 GHz, as shown in Fig. 11(b). The measured 20-dB bandwidth of the bandstop filter response is ~100 MHz. However, the 3-dB bandwidth is still in the order of 3 GHz, limited by the broad resonance of the ring resonance. It should be noted that the filter response around 3 GHz shown in Fig. 11(b) exhibits a higher passband loss because the ring's extended phase response is close to the optical carrier and therefore simultaneously disturbs phases of the optical carrier and the processed sideband. As a result, these undesirable phase variations lead to imperfect constructive RF signal interference at the passband frequencies. The filter bandwidth can be further narrowed down by using a wider waveguide width with a lower round-trip loss of the ring resonator.[40] Alternatively, through the hybrid integration technology,[48,55,56] ultralow-loss Si or Si_3N_4 ring resonators that are heterogeneously integrated with Brillouin-active circuits can offer high-resolution linear filtering. The filter rejection and shape of the bandstop filter response can also be improved by optimizing the broadband SBS pump envelope, in conjunction with the increased SBS gain.

C. Link performance optimization and analysis

An important feature of the filter scheme implemented in this work is the compatibility with the well-developed link performance optimization techniques, typically low-biased intensity modulation in an optically amplified MWP link.[57,58] Since the low-biasing operation only varies the optical carrier-to-sideband ratio without changing the phase relation, the notch filter formation will not be affected during the link optimization process.

Following the optimization approach by lowering the modulator DC bias angle,[33] the RF link gain in the MWP filter passband was optimized to a maximum level of −6 dB at 1 GHz, as shown in Fig. 12(a). Meanwhile, the deep filter suppression and center frequency tunability are both perfectly maintained, demonstrating the fact that the notch filter formation is decoupled from the link performance optimization process. This feature allows for achieving simultaneous optimization of advanced filter functionality and enhanced RF link performance. The roll-off baseline of the measured filter response is due to the increased RF losses of the electric components at higher RF frequencies.

To present the overall RF link performance, the RF link gain, noise figure, and spuriousfree dynamic range (SFDR) were characterized for a filter with a notch frequency around 9 GHz. As shown in Fig. 12(b), in general, the average RF link gain is in the level of −10 dB in the filter passband. The RF link gain reduces to the level of < −30 dB around 9 GHz, indicating the notch frequency of the RF filter. The RF link gain in the current demonstration is limited by the relative high insertion loss of the photonic waveguide (18 dB). By optimizing the circuit design and fabrication process, the total insertion loss can be reduced to the level of 10 dB which is the typical insertion loss of integrated As_2S_3 photonic circuits.[50] The measured noise figure is in the range from 20 dB to 30 dB in the passband. The noise figure is mainly affected by the RF link loss and the detected electrical noises. In the measurement, the photocurrent of 7.97 mA yields a measured noise power spectral density (PSD) of −157 dBm/Hz at frequencies >1 GHz, much higher than the thermal noise floor of −174 dBm/Hz.

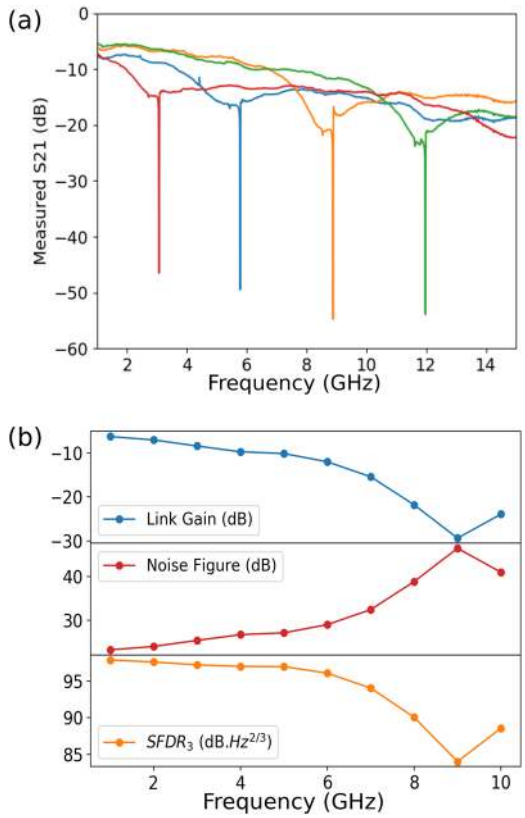

FIG. 12. Measured results of (a) MWP filter response at different center frequencies with an optimized link performance and (b) overall link performance of a notch filter response around 9 GHz.

The spuriousfree dynamic range (SFDR) is an important figure of merit to quantify the impact of the signal distortions induced by the system response nonlinearity. The $SFDR_n$ indicates the maximum output signal-to-noise ratio, without the need for additional filtering to eliminate the *n*th-order intermodulation frequency components. As shown in Fig. 12(b), the measured $SFDR_3$ in the filter passband is typically >96 dB $Hz^{2/3}$. To analyze the SFDR, we take a representative SFDR measurement at the passband frequency of 5 GHz of a notch filter with a notch frequency around 9 GHz. The filter passband yields a link gain of −10.1 dB, a noise figure of 27.1 dB, and a $SFDR_3$ of 96.5 dB $Hz^{2/3}$, as shown in Fig. 13(a). The $SFDR_3$ is mainly limited by the relatively high 3rd distortion, which is indicated by the low 3rd-order input intercept point (IIP_3) denoted in Fig. 13(a). The measured IIP_3 is −2.2 dBm which is much lower than the reported 19 dBm for the IMWP filters without using RF amplifiers.[51] The reduction in IIP_3 is mainly attributed to the use of an RF amplifier prior to the modulator, which increases the 3rd-order distortion in the MWP filter link. In the future work, the use of the lower-loss photonic circuits can eliminate the need for RF amplifiers for link loss compensation to the same level of performance reported in reported demonstration.[51] The high $SFDR_2$ originates from the low-biased intensity modulator which operates in a less linear modulation regime. However, the 2nd-order distortion will not be problematic for suboctave RF applications, since the 2nd-order distortions can be easily filtered out.

To further reduce the noise figure, it is necessary to analyze the dominant noise contributions. In the experiment, we found that the majority of the detected electrical noise is caused by the back-reflected optical pump. In the measurement, the photocurrent contributed from the transmitted optical signal is merely ~0.55 mA (1 mW × 0.55 A/W), while the total photocurrent of 7.97 mA when the optical pump was switched on. The increased photocurrent was mainly contributed by the reflected pump at the chip facet and the amplified signal by the SBS gain process. In the experiment, the total received power including the back reflection is nearly linear to the pump power, when the input Brillouin pump power was more than 100 mW. This excessive pump reflection leads to a large degradation of noise figure by more than 10 dB due to the increase in the detected electrical noise power, while the RF link gain remains unchanged. To understand the link performance degradation caused by the reflected optical pump, we calculated the $SFDR_3$ for the case when the optical pump was turned off. In this case, the RF notch filter response is formed by only the OC ring resonator. As a comparison, the $SFDR_3$ when the pump was on is shown in Fig. 13.

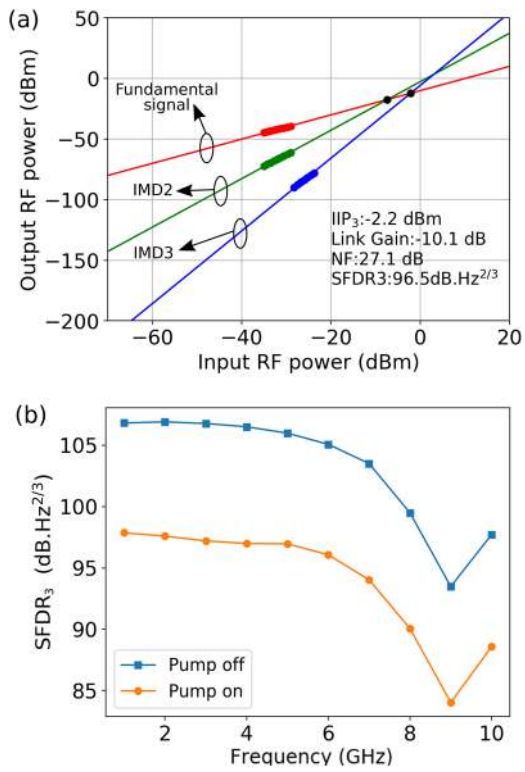

FIG. 13. Measured results of (a) two-tone test in the filter passband at 5 GHz and (b) $SFDR_3$ comparisons with and without the existence of the SBS pump back reflection to the photodetector.

From the comparison, the difference in $SFDR_3$ between SBS pump on and off is around 9.5 dB, indicating a significant passband gain deterioration by the reflected optical. In the future development, the pump back-reflection must have to be minimized to decrease the noise figure. Possible approaches include the use of antireflection coating at the chip facet. The recently demonstrated intermodal SBS schemes[59,60] also provide a feasible to separate the processed signal from the reflected optical pump, since the pump and signal waves use separate input/output ports.

The reported platform can also be extended to the implementation of an RF bandpass filter,[61,62] since the synthesized transfer function can flip the optical sideband phase by 180° without altering the amplitude. Therefore, phase-modulated out-of-phase sidebands can be converted into an equivalent intensity modulation within a narrow spectral range, forming an RF passband over the selective range. On the contrary, the other unchanged sideband frequencies undergo destructive interference that produces broad RF stopbands. In this case, the RF link gain of the bandpass filter is expected to achieve the same level of the performance reported in the notch filter due to the constructive RF interference. However, the noise power at RF passband frequencies will possibly increase owing to the additional noise generated by the SBS Stokes (gain) process.

Alternative approaches can be used to implement desirable π-phase-shift-only response, such as the transparent SBS response scheme based on the superposition of slightly frequency-detuned Brillouin gain and loss responses.[63,64] However, the residual gain and loss response near the gain transparency frequencies will distort the resultant RF filter response. Moreover, the optical pump power required for achieving the Brillouin-induced π-phase shift is very likely to exceed the power handling capability of the integrated photonic chip, especially for the case where broadband transparent response is needed.

V. CONCLUSION

In this work, we show a high-performance integrated microwave photonic notch filter based on the novel concept of pairing linear with nonlinear optical circuits on the same photonic chip. To demonstrate this concept, we implemented a chip-based RF photonic notch filter using an As_2S_3 photonic circuit that simultaneously integrates linear ring resonators with Brillouin-active waveguides. The demonstrated chip-based RF photonic notch filter, for the first time, merges demanding features including ultradeep suppression, wideband and simple frequency tunability, filter-shape programmability, and the compatibility with existing link performance techniques and compactness. We discussed how to further improve the filter performance by means of reducing the chip insertion loss and the pump reflection. This work establishes a novel approach to designing and implementing high-performance IMWP systems for portable and space RF applications, with all-optimized performance and functionality.

ACKNOWLEDGMENTS

This work was supported by Lockheed Martin under the University of Sydney contract.

REFERENCES

[1]A. E. Willner, O. F. Yilmaz, J. Wang, X. Wu, A. Bogoni, L. Zhang, and S. R. Nuccio, "Optically efficient nonlinear signal processing," IEEE J. Sel. Top. Quantum Electron. **17**, 320–322 (2011).

[2]D. Marpaung, M. Pagani, B. Morrison, and B. J. Eggleton, "Nonlinear integrated microwave photonics," J. Lightwave Technol. **32**, 3421–3427 (2014); e-print arXiv:1310.4897.

[3]D. Marpaung, J. Yao, and J. Capmany, "Integrated microwave photonics," Nat. Photonics **13**, 80–90 (2019).

[4]W. Liang, D. Eliyahu, V. S. Ilchenko, A. A. Savchenkov, A. B. Matsko, D. Seidel, and L. Maleki, "High spectral purity Kerr frequency comb radio frequency photonic oscillator," Nat. Commun. **6**, 7957 (2015).

[5]J. Li, H. Lee, and K. J. Vahala, "Microwave synthesizer using an on-chip Brillouin oscillator," Nat. Commun. **4**, 2097 (2013).

[6]M. Zhang, B. Buscaino, C. Wang, A. Shams-Ansari, C. Reimer, R. Zhu, J. M. Kahn, and M. Lončar, "Broadband electro-optic frequency comb generation in a lithium niobate microring resonator," Nature **568**, 373–377 (2019); e-print arXiv:1809.08636.

[7]C. Wang, M. Zhang, M. Yu, R. Zhu, H. Hu, and M. Loncar, "Monolithic lithium niobate photonic circuits for Kerr frequency comb generation and modulation," Nat. Commun. **10**, 978 (2019).

[8]M. Pagani, B. Morrison, Y. Zhang, A. Casas-Bedoya, T. Aalto, M. Harjanne, M. Kapulainen, B. J. Eggleton, and D. Marpaung, "Low-error and broadband microwave frequency measurement in a silicon chip," Optica **2**, 751 (2015).

[9]Z. Zhu, M. Merklein, D.-Y. Choi, K. Vu, P. Ma, S. J. Madden, and B. J. Eggleton, "Highly sensitive, broadband microwave frequency identification

using a chip-based Brillouin optoelectronic oscillator," Opt. Express **27**, 12855 (2019).
[10]X. Xue, Y. Xuan, H. J. Kim, J. Wang, D. E. Leaird, M. Qi, and A. M. Weiner, "Programmable single-bandpass photonic RF filter based on Kerr comb from a microring," J. Lightwave Technol. **32**, 3557–3565 (2014).
[11]X. Xu, M. Tan, J. Wu, T. G. Nguyen, S. T. Chu, B. E. Little, R. Morandotti, A. Mitchell, and D. J. Moss, "High performance RF filters via bandwidth scaling with Kerr micro-combs," APL Photonics **4**, 026102 (2019).
[12]G. P. Agrawal, *Nonlinear Fiber Optics*, 2nd ed. (Academic Press, San Diego, CA, 1989).
[13]E. Ippen and R. Stolen, "Stimulated Brillouin scattering in optical fibers," Appl. Phys. Lett. **21**, 539–541 (1972).
[14]A. Kobyakov, M. Sauer, and D. Chowdhury, "Stimulated Brillouin scattering in optical fibers," Adv. Opt. Photonics **2**, 1 (2010).
[15]B. J. Eggleton, C. G. Poulton, and R. Pant, "Inducing and harnessing stimulated Brillouin scattering in photonic integrated circuits," Adv. Opt. Photonics **5**, 536 (2013).
[16]R. Van Laer, B. Kuyken, D. Van Thourhout, and R. Baets, "Interaction between light and highly confined hypersound in a silicon photonic nanowire," Nat. Photonics **9**, 199–203 (2015); e-print arXiv:1407.4977.
[17]E. A. Kittlaus, H. Shin, and P. T. Rakich, "Large Brillouin amplification in silicon," Nat. Photonics **10**, 463–467 (2016).
[18]D. Marpaung, B. Morrison, M. Pagani, R. Pant, D.-Y. Choi, B. Luther-Davies, S. J. Madden, and B. J. Eggleton, "Low-power, chip-based stimulated Brillouin scattering microwave photonic filter with ultrahigh selectivity," Optica **2**, 76 (2015).
[19]A. Casas-Bedoya, B. Morrison, M. Pagani, D. Marpaung, and B. J. Eggleton, "Tunable narrowband microwave photonic filter created by stimulated Brillouin scattering from a silicon nanowire," Opt. Lett. **40**, 4154 (2015); e-print arXiv:1506.07637v1.
[20]E. A. Kittlaus, P. Kharel, N. T. Otterstrom, Z. Wang, and P. T. Rakich, "RF-photonic filters via on-chip photonic–phononic emit–receive operations," J. Lightwave Technol. **36**, 2803–2809 (2018); e-print arXiv:1801.00750.
[21]A. Choudhary, Y. Liu, D. Marpaung, and B. Eggleton, "On-chip Brillouin filtering of RF and optical signals," IEEE J. Sel. Top. Quantum Electron. **24**, 1–11 (2018).
[22]Y. Liu, D. Marpaung, B. J. Eggleton, and A. Choudhary, "High-performance chip-assisted microwave photonic functionalities," IEEE Photonics Technol. Lett. **30**, 1822–1825 (2018).
[23]I. Aryanfar, D. Marpaung, A. Choudhary, Y. Liu, K. Vu, D.-Y. Choi, P. Ma, S. Madden, and B. J. Eggleton, "Chip-based Brillouin radio frequency photonic phase shifter and wideband time delay," Opt. Lett. **42**, 1313 (2017).
[24]Y. Liu, A. Choudhary, D. Marpaung, and B. J. Eggleton, "Chip-based Brillouin processing for phase control of RF signals," IEEE J. Quantum Electron. **54**, 1–13 (2018).
[25]M. Pagani, D. Marpaung, D.-Y. Choi, S. J. Madden, B. Luther-Davies, and B. J. Eggleton, "Tunable wideband microwave photonic phase shifter using on-chip stimulated Brillouin scattering," Opt. Express **22**, 28810 (2014).
[26]L. McKay, M. Merklein, A. C. Bedoya, A. Choudhary, M. Jenkins, C. Middleton, A. Cramer, J. Devenport, A. Klee, R. DeSalvo, and B. J. Eggleton, "Brillouin-based phase shifter in a silicon waveguide," Optica **6**, 907 (2019); e-print arXiv:1903.08363.
[27]M. Merklein, B. Stiller, I. V. Kabakova, U. S. Mutugala, K. Vu, S. J. Madden, B. J. Eggleton, and R. Slavík, "Widely tunable, low phase noise microwave source based on a photonic chip," Opt. Lett. **41**, 4633 (2016).
[28]D. Marpaung, B. Morrison, R. Pant, and B. J. Eggleton, "Frequency agile microwave photonic notch filter with anomalously high stopband rejection," Opt. Lett. **38**, 4300–4303 (2013); e-print arXiv:1308.1146.
[29]A. N. Tait, M. A. Nahmias, B. J. Shastri, and P. R. Prucnal, "Broadcast and weight: An integrated network for scalable photonic spike processing," J. Lightwave Technol. **32**, 4029–4041 (2014).
[30]M. Burla, D. Marpaung, L. Zhuang, C. Roeloffzen, M. R. Khan, A. Leinse, M. Hoekman, and R. Heideman, "On-chip CMOS compatible reconfigurable optical delay line with separate carrier tuning for microwave photonic signal processing," Opt. Express **19**, 21475 (2011).
[31]W. Bogaerts, P. De Heyn, T. Van Vaerenbergh, K. De Vos, S. Kumar Selvaraja, T. Claes, P. Dumon, P. Bienstman, D. Van Thourhout, and R. Baets, "Silicon microring resonators," Laser Photonics Rev. **6**, 47–73 (2012).
[32]Y. Liu, A. Choudhary, D. Marpaung, and B. J. Eggleton, "Gigahertz optical tuning of an on-chip radio frequency photonic delay line," Optica **4**, 418 (2017).
[33]Y. Liu, D. Marpaung, A. Choudhary, and B. J. Eggleton, "Lossless and high-resolution RF photonic notch filter," Opt. Lett. **41**, 5306 (2016).
[34]Y. Liu, A. Choudhary, G. Ren, K. Vu, B. Morrison, A. Casas-Bedoya, T. G. Nguyen, D. Choi, A. Mitchell, S. J. Madden, D. Marpaung, and B. J. Eggleton, "Integrating Brillouin processing with functional circuits for enhanced RF photonic processing," in *2018 International Topical Meeting on Microwave Photonics (MWP)* (IEEE, 2018), pp. 1–4.
[35]Y. Liu, "High-performance on-chip microwave photonic signal processing using linear and nonlinear optics," Ph.D. thesis, University of Sydney, 2019.
[36]C. G. Poulton, R. Pant, and B. J. Eggleton, "Acoustic confinement and stimulated Brillouin scattering in integrated optical waveguides," J. Opt. Soc. Am. B **30**, 2657–2664 (2013); e-print arXiv:1308.0382.
[37]A. H. Safavi-Naeini, D. Van Thourhout, R. Baets, and R. Van Laer, "Controlling phonons and photons at the wavelength scale: Integrated photonics meets integrated phononics," Optica **6**, 213 (2019); e-print arXiv:1810.03217.
[38]B. C. P. Sturmberg, K. B. Dossou, M. J. A. Smith, B. Morrison, C. G. Poulton, and M. J. Steel, "Finite element analysis of stimulated Brillouin scattering in integrated photonic waveguides," J. Lightwave Technol. **37**, 3791–3804 (2019).
[39]M. J. A. Smith, B. T. Kuhlmey, C. M. de Sterke, C. Wolff, M. Lapine, and C. G. Poulton, "Metamaterial control of stimulated Brillouin scattering," Opt. Lett. **41**, 2338 (2016); e-print arXiv:1602.03222.
[40]G. Li, J. Yao, H. Thacker, A. Mekis, X. Zheng, I. Shubin, Y. Luo, J.-h. Lee, K. Raj, J. E. Cunningham, and A. V. Krishnamoorthy, "Ultralow-loss, high-density SOI optical waveguide routing for macrochip interconnects," Opt. Express **20**, 12035 (2012).
[41]M. Á. Guillén-Torres, K. Murray, H. Yun, M. Caverley, E. Cretu, L. Chrostowski, and N. A. F. Jaeger, "Effects of backscattering in high-Q, large-area silicon-on-insulator ring resonators," Opt. Lett. **41**, 1538 (2016).
[42]S. A. Miller, M. Yu, X. Ji, A. G. Griffith, J. Cardenas, A. L. Gaeta, and M. Lipson, "Low-loss silicon platform for broadband mid-infrared photonics," Optica **4**, 707 (2017); e-print arXiv:1703.03517.
[43]Y. Liu, T. Chang, and A. E. Craig, "Coupled mode theory for modeling microring resonators," Opt. Eng. **44**, 084601 (2005).
[44]L. Chrostowski and M. Hochberg, *Silicon Photonics Design* (Cambridge University Press, Cambridge, 2015).
[45]W.-P. Huang, "Coupled-mode theory for optical waveguides: An overview," J. Opt. Soc. Am. A **11**, 963 (1994).
[46]S. J. Madden, D.-Y. Choi, D. A. Bulla, A. V. Rode, B. Luther-Davies, V. G. Ta'eed, M. D. Pelusi, and B. J. Eggleton, "Long, low loss etched As_2S_3 chalcogenide waveguides for all-optical signal regeneration," Opt. Express **15**, 14414 (2007).
[47]M. Cherchi, S. Ylinen, M. Harjanne, M. Kapulainen, and T. Aalto, "Dramatic size reduction of waveguide bends on a micron-scale silicon photonic platform," Opt. Express **21**, 17814 (2013).
[48]B. Morrison, A. Casas-Bedoya, G. Ren, K. Vu, Y. Liu, A. Zarifi, T. G. Nguyen, D.-Y. Choi, D. Marpaung, S. J. Madden, A. Mitchell, and B. J. Eggleton, "Compact Brillouin devices through hybrid integration on silicon," Optica **4**, 847 (2017); e-print arXiv:1702.05233.
[49]Y. Liu, D. Marpaung, A. Choudhary, and B. J. Eggleton, "Lossless and high-resolution RF photonic filter," in *2016 IEEE Avionics and Vehicle Fiber-Optics and Photonics Conference (AVFOP)* (IEEE, 2016), Vol. 41, pp. 185–186.
[50]A. Choudhary, B. Morrison, I. Aryanfar, S. Shahnia, M. Pagani, Y. Liu, K. Vu, S. Madden, D. Marpaung, and B. J. Eggleton, "Advanced integrated microwave signal processing with giant on-chip Brillouin gain," J. Lightwave Technol. **35**, 846–854 (2017).
[51]Y. Liu, J. Hotten, A. Choudhary, B. J. Eggleton, and D. Marpaung, "All-optimized integrated RF photonic notch filter," Opt. Lett. **42**, 4631 (2017).
[52]M. Rasras, K.-Y. Tu, D. Gill, Y.-K. Chen, A. White, S. Patel, A. Pomerene, D. Carothers, J. Beattie, M. Beals, J. Michel, and L. Kimerling, "Demonstration of

a tunable microwave-photonic notch filter using low-loss silicon ring resonators," J. Lightwave Technol. **27**, 2105–2110 (2009).
[53]A. Zadok, O. Raz, A. Eyal, and M. Tur, "Optically controlled low-distortion delay of GHz-wide radio-frequency signals using slow light in fibers," IEEE Photonics Technol. Lett. **19**, 462–464 (2007).
[54]W. Wei, L. Yi, Y. Jaouen, M. Morvan, and W. Hu, "Brillouin rectangular optical filter with improved selectivity and noise performance," IEEE Photonics Technol. Lett. **27**, 1593–1596 (2015).
[55]R. Califa, D. Munk, H. Genish, Y. Kaganovskii, I. Bakish, M. Rosenbluh, and A. Zadok, "Large one-time photo-induced tuning of directional couplers in chalcogenide-on-silicon platform," Opt. Express **23**, 28234 (2015).
[56]B. Shen, H. Lin, F. Merget, S. S. Azadeh, C. Li, G.-Q. Lo, K. A. Richardson, J. Hu, and J. Witzens, "Broadband couplers for hybrid silicon-chalcogenide glass photonic integrated circuits," Opt. Express **27**, 13781 (2019).
[57]V. J. Urick, M. E. Godinez, P. S. Devgan, J. D. McKinney, and F. Bucholtz, "Analysis of an analog fiber-optic link employing a low-biased Mach-Zehnder modulator followed by an erbium-doped fiber amplifier," J. Lightwave Technol. **27**, 2013–2019 (2009).
[58]Y. Liu, D. Marpaung, A. Choudhary, J. Hotten, and B. J. Eggleton, "Link performance optimization of chip-based Si_3N_4 microwave photonic filters," J. Lightwave Technol. **36**, 4361–4370 (2018).
[59]E. A. Kittlaus, N. T. Otterstrom, and P. T. Rakich, "On-chip inter-modal Brillouin scattering," Nat. Commun. **8**, 15819 (2017); e-print arXiv:1611.03556.
[60]Y. Liu, A. Choudhary, G. Ren, D.-Y. Choi, A. Casas-Bedoya, B. Morrison, P. Ma, T. G. Nguyen, K. Vu, A. Mitchell, S. J. Madden, D. Marpaung, and B. J. Eggleton, "On-chip backward inter-modal Brillouin scattering," in *Conference on Lasers and Electro-Optics* (OSA Technical Digest, Optical Society of America, 2019), Vol. 1, p. STh1J.4.
[61]A. Byrnes, R. Pant, E. Li, D.-Y. Choi, C. G. Poulton, S. Fan, S. Madden, B. Luther-Davies, and B. J. Eggleton, "Photonic chip based tunable and reconfigurable narrowband microwave photonic filter using stimulated Brillouin scattering," Opt. Express **20**, 18836 (2012).
[62]A. Choudhary, I. Aryanfar, S. Shahnia, B. Morrison, K. Vu, S. Madden, B. Luther-Davies, D. Marpaung, and B. J. Eggleton, "Tailoring of the Brillouin gain for on-chip widely tunable and reconfigurable broadband microwave photonic filters," Opt. Lett. **41**, 436 (2016).
[63]J. Liu, X. Wu, C. Huang, H. K. Tsang, and C. Shu, "Compensation of dispersion-induced power fading in analog photonic links by gain-transparent SBS," IEEE Photonics Technol. Lett. **30**, 688–691 (2018).
[64]A. Loayssa and F. J. Lahoz, "Broad-band RF photonic phase shifter based on stimulated Brillouin scattering and single-sideband modulation," IEEE Photonics Technol. Lett. **18**, 208–210 (2006).